# Experimental and Numerical Characterization of a Steady-State Cylindrical Blackbody Cavity at 1100 Degrees Celsius

*Thomas J. Horn*
*NASA Dryden Flight Research Center*
*Edwards, California*

*Amanie N. Abdelmessih*
*Saint Martin's College*
*Lacey, Washington*

**August 2000**

# The NASA STI Program Office…in Profile

Since its founding, NASA has been dedicated to the advancement of aeronautics and space science. The NASA Scientific and Technical Information (STI) Program Office plays a key part in helping NASA maintain this important role.
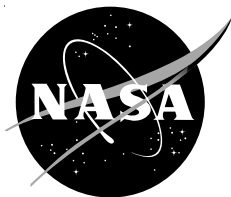
The NASA STI Program Office is operated by Langley Research Center, the lead center for NASA's scientific and technical information. The NASA STI Program Office provides access to the NASA STI Database, the largest collection of aeronautical and space science STI in the world. The Program Office is also NASA's institutional mechanism for disseminating the results of its research and development activities. These results are published by NASA in the NASA STI Report Series, which includes the following report types:

- TECHNICAL PUBLICATION. Reports of completed research or a major significant phase of research that present the results of NASA programs and include extensive data or theoretical analysis. Includes compilations of significant scientific and technical data and information deemed to be of continuing reference value. NASA's counterpart of peer-reviewed formal professional papers but has less stringent limitations on manuscript length and extent of graphic presentations.

- TECHNICAL MEMORANDUM. Scientific and technical findings that are preliminary or of specialized interest, e.g., quick release reports, working papers, and bibliographies that contain minimal annotation. Does not contain extensive analysis.

- CONTRACTOR REPORT. Scientific and technical findings by NASA-sponsored contractors and grantees.

- CONFERENCE PUBLICATION. Collected papers from scientific and technical conferences, symposia, seminars, or other meetings sponsored or cosponsored by NASA.

- SPECIAL PUBLICATION. Scientific, technical, or historical information from NASA programs, projects, and mission, often concerned with subjects having substantial public interest.

- TECHNICAL TRANSLATION. English-language translations of foreign scientific and technical material pertinent to NASA's mission.

Specialized services that complement the STI Program Office's diverse offerings include creating custom thesauri, building customized databases, organizing and publishing research results…even providing videos.

For more information about the NASA STI Program Office, see the following:

- Access the NASA STI Program Home Page at ***http://www.sti.nasa.gov***

- E-mail your question via the Internet to help@sti.nasa.gov

- Fax your question to the NASA Access Help Desk at (301) 621-0134

- Telephone the NASA Access Help Desk at (301) 621-0390

- Write to:
  NASA Access Help Desk
  NASA Center for AeroSpace Information
  7121 Standard Drive
  Hanover, MD 21076-1320

NASA/TM-2000-209022

# Experimental and Numerical Characterization of a Steady-State Cylindrical Blackbody Cavity at 1100 Degrees Celsius

*Thomas J. Horn*
*NASA Dryden Flight Research Center*
*Edwards, California*

*Amanie N. Abdelmessih*
*Saint Martin's College*
*Lacey, Washington*

**August 2000**

Available from the following:

# EXPERIMENTAL AND NUMERICAL CHARACTERIZATION OF A STEADY-STATE CYLINDRICAL BLACKBODY CAVITY AT 1100 DEGREES CELSIUS

**Thomas J. Horn**
Aerostructures Branch
NASA Dryden Flight Research Center
P.O. Box 273, MS 48202A
Edwards, California 93523
Tel (661) 276-2232, Fax (661) 276-2852, tom.horn@dfrc.nasa.gov


**Amanie N. Abdelmessih, Ph. D.**
Associate Professor
Mechanical Engineering Department
Saint Martin's College
5300 Pacific Avenue SE
Lacey, Washington 98503-1297
Tel (360) 438-4532, Fax (360) 438-4548, abdelmessih@stmartin.edu

**KEYWORDS:** Blackbody calibration furnace, Heat flux calibration, Heat transfer, Numerical thermal analysis, Temperature measurement.

## ABSTRACT

A blackbody calibration furnace at the NASA Dryden Flight Research Center is used to calibrate heat flux gages. These gages are for measuring the aerodynamic heat flux on hypersonic flight vehicle surfaces. The blackbody is a graphite tube with a midplane partition which divides the tube into two compartments (dual cavities). Electrical resistance heating is used to heat the graphite tube. This heating and the boundary conditions imposed on the graphite tube result in temperature gradients along the walls of the blackbody cavity. This paper describes measurements made during steady-state operation and development of finite-difference thermal models of the blackbody furnace at 1100 °C. Two configurations were studied, one with the blackbody outer surface insulated and the other without insulation. The dominant modes of heat transfer were identified for each configuration and the effect of variations in material properties and electric current that was passed through the blackbody were quantified.

## NOMENCLATURE

| | |
|---|---|
| A | area, mm$^2$ |
| ATJ | an isostatically molded grade of graphite with fine grain and high strength |
| E | emissive power, W/m$^2$ |
| $F$ | emissive power scaling factor |
| FLL | Flight Loads Laboratory at NASA Dryden Flight Research Center, Edwards, California |
| I | electric current, amperes |
| kW | kilowatt |
| L | length, mm |
| MPa | megapascal |
| MW | megawatt |
| NASA | National Aeronautics and Space Administration |
| NIST | National Institute of Standards and Technology |

| OFT | optical fiber thermometer |
|---|---|
| P | power, watts |
| PID | proportional integral derivative |
| R | electrical resistance, ohm |
| T | absolute temperature, K |
| V | volume, mm$^3$ |
| W | watt |
| x | distance from center partition, mm |
| $\Delta T$ | temperature change |
| $\rho$ | electrical resistivity, ohm·mm |
| $\sigma$ | Stefan-Boltzman constant, $5.670 \times 10^{-8}$ W·m$^{-2}$·K$^{-4}$ |

**Subscripts:**

| corr | corrected |
|---|---|
| ind | optical fiber thermometer indicated reading |
| ref | reference pyrometer |
| tot | total |

## INTRODUCTION

During hypersonic flight, high heat fluxes are generated on the surfaces of vehicles. It is important to understand what these heat fluxes are in order to better understand the aerodynamics of hypersonic flight. Heat flux gages can be used to measure these heat fluxes but they need to be properly calibrated before they are put into service. In addition, the furnace used to calibrate these gages must be characterized in order to determine its effect on the accuracy of the calibration.

The National Institute of Standards and Technology (NIST), Gaithersburg, Maryland, has made significant strides in recent years towards developing well-understood calibration systems which operate in convection, conduction, and radiation heat transfer modes (Holmberg, et al., 1997; Grosshandler and Blackburn, 1997; Murthy, et al., 1997; Holmberg, et al., 1999). The most powerful of the NIST facilities is a radiation facility capable of producing heat fluxes of 200 kW/m$^2$. This is still well below the heat fluxes that can be generated in hypersonic flight, which can be in excess of 1 MW/m$^2$.

The Flight Loads Laboratory (FLL) at NASA's Dryden Flight Research Center, Edwards, California is equipped with a calibration furnace capable of calibrating heat flux gages up to 1.1 MW/m$^2$ and temperature sensors of up to 2200 °C. This calibration system uses a cylindrical dual-cavity blackbody for calibrating a reference heat flux gage. It can also be fitted with a flat plate heating element to calibrate heat flux gages (having geometries that can not be inserted into the blackbody cavity) against the reference heat flux gage. The calibration furnace manufacturer (Thermogage, 1991) recommends that the blackbody temperature at the center of the middle partition be measured with a NIST traceable optical pyrometer, then the heat flux gage can be inserted into the blackbody cavity for a few seconds. The calibration of the heat flux gage is determined by dividing the emissive power of the blackbody by the peak output generated by the heat flux gage during the insertion. This process may be repeated at other temperatures (and hence heat fluxes) as required.

There are two key questions which must be answered in order to produce a quality heat flux gage calibration with well-defined uncertainty intervals. First, what effect do the various boundary conditions (such as conduction, radiation, convection, and the effect of axial temperature gradients) have on the blackbody cavity (Abdelmessih, 1998). Secondly, what effect does the presence of the reference heat flux gage in the blackbody cavity have on the calibration. The measurement uncertainties associated with these questions have not been specifically addressed in the literature and no detailed thermal analysis has been performed. Therefore, it is the purpose of this work to establish the basis of addressing these questions.

Research at the FLL aimed at quantifying the uncertainties associated with this calibration system and process has begun by performing experimental and numerical characterization of both the blackbody cavity (which is discussed in this paper) and the flat plate heater (Jiang, et al., 1998). Proper characterization of the system will require transient analyses of the reference heat flux gage insertion process.

This paper discusses the initial efforts to characterize the blackbody cavity under steady-state operations at 1100 °C. These efforts include detailed experimental measurements and two-dimensional, axisymmetric, numerical, thermal models. The temperature of 1100 °C was chosen because it is the temperature at which the heat flux calibration system manufacturer recommends switching from the uninsulated blackbody configuration used at lower temperatures to the insulated configuration used at higher temperatures. The steady-state models will help quantify the relative importance of the various boundary conditions present in the blackbody system. They will also serve as an important step towards a transient analysis defining both the relevant physical phenomena and the initial conditions required at the start of a transient thermal analyses.
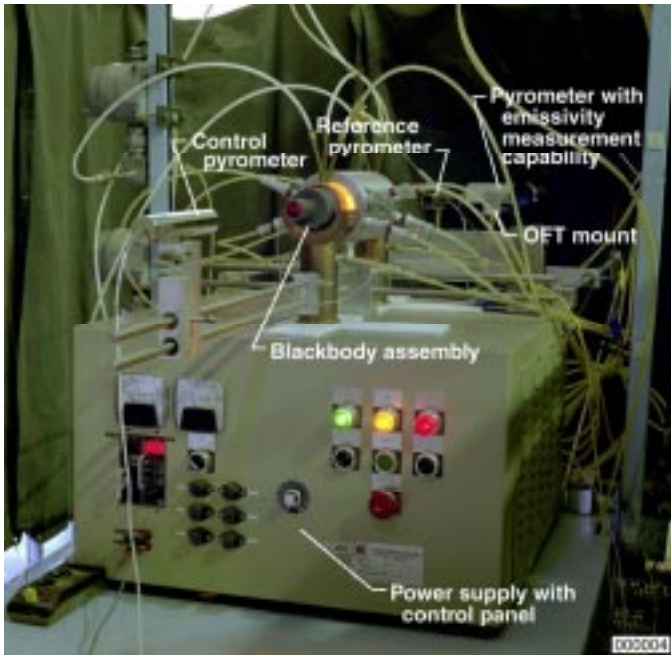
Note that use of trade names or names of manufacturers in this document does not constitute an official endorsement of such products or manufacturers, either expressed or implied, by the National Aeronautics and Space Administration.

## EXPERIMENTAL OVERVIEW

Various experimental measurements were made as part of the blackbody calibration system characterization process. This section describes the calibration system hardware, the instrumentation used to acquire the various measurements, and the procedures used during testing.
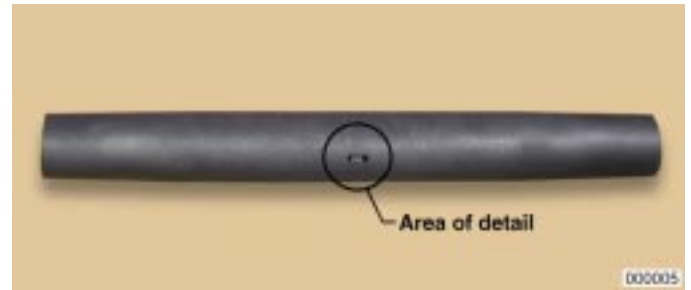
### Test Setup

Figure 1 shows the calibration system. This system consists of a power supply, a dual-cavity cylindrical blackbody, and an
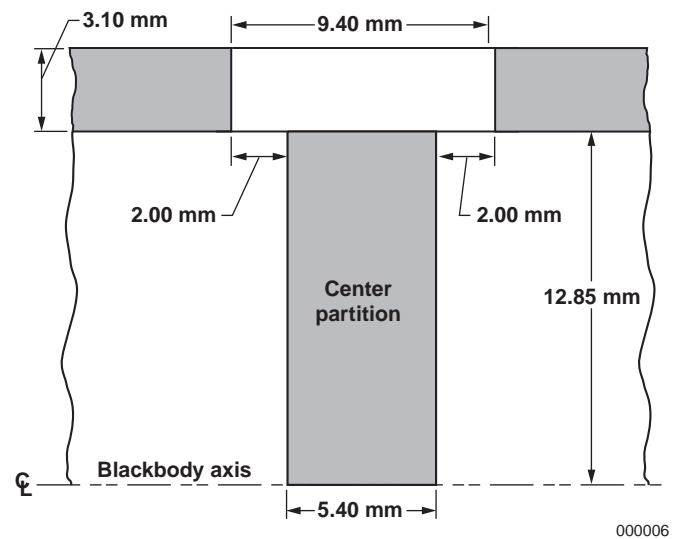
Figure 1.   Blackbody Calibration Furnace.



Figure 2(a). Overview.



Figure 2(b).  Partition Detail.

Figure 2.   Graphite Blackbody Tube (dual cavities).



Figure 3.   Blackbody Assembly Components.

optical pyrometer for temperature control which views one side of the partition in the graphite tube. Other components not shown in the figure include a computer used for data acquisition and temperature control, a cooling system, and a supply of compressed argon gas.

The blackbody cavity (Fig. 2a) is a hollow cylinder measuring 25.7 mm inside diameter. It is manufactured from ATJ graphite and is 28.9 cm long, with a 5.4-mm-thick partition at the middle. ATJ is an isostatically-molded grade of graphite of fine grain and high strength. At the top center of the graphite tube is an oval slot (Fig. 2b) that is 9.4 mm long by 3.1 mm wide and serves as a bleed port for argon purge gas during pretest purging of the blackbody cavities. The graphite tube is assembled with other components, shown in Fig. 3. This graphite tube is held in place at each end by a graphite bushing assembly installed in a copper ring (Fig. 4). A quartz tube, which serves as a containment barrier for argon purge gas, is held between the copper rings. The space between the outer surface of the blackbody and the quartz tube is insulated with graphite felt and foil when temperatures at 1100 °C or above are desired. This space is left uninsulated when the temperature does not exceed 1100 °C. Unheated graphite extension tubes, 15.2 cm long, are installed at both ends. Laminar flow of argon gas exiting the extension tubes prevents air from diffusing into the heated graphite tube.
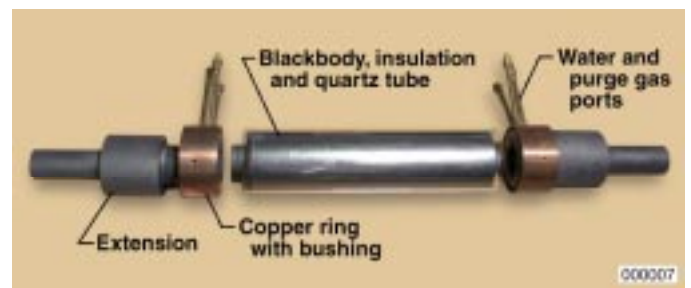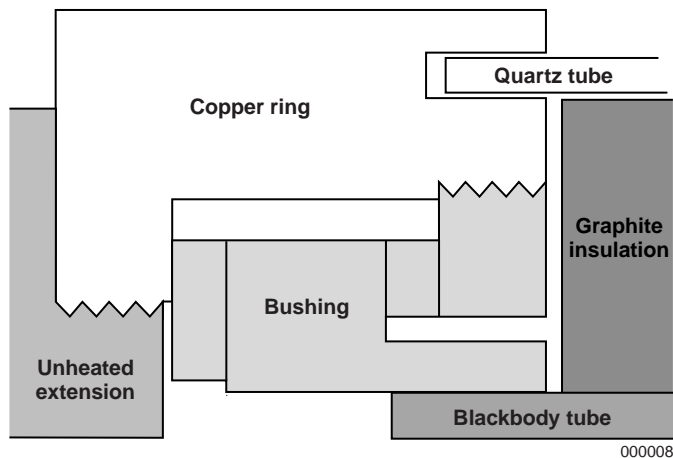
**Figure 4.  Copper Ring and Bushing Detail.**

Figure 5 shows this entire assembly placed atop two electrodes that are connected to the power supply. Stable temperatures between 800 °C and 2200 °C can be attained at the center of the graphite tube by passing regulated electric current from the power supply through the blackbody assembly. The copper electrodes and rings which hold the blackbody assembly are water cooled. An aluminum water-cooled reflector (Fig. 5) surrounds the quartz cylinder. This reflector serves as the radiation boundary for the external surface of the graphite tube during tests run without graphite insulation in the quartz cylinder, thereby reducing heat lost to the ambient surroundings and ensuring more uniform temperatures in the blackbody cavity. The reflector is left in place during insulated runs as a safety device to prevent contact with potentially hot surfaces.

To minimize oxidation of the graphite, argon is used to purge the interior and exterior of the graphite tube. The argon is introduced through ports in the copper rings at each end of the tube. The argon is forced into the blackbody cavity before heating, as well as into the space between the graphite tube and



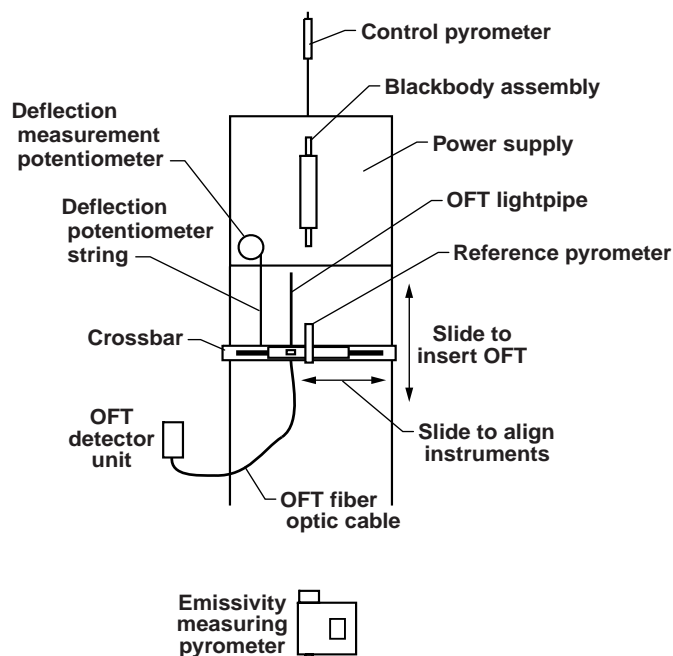**Figure 5.  Assembled Blackbody on Electrodes.**

quartz tube, including the insulation when installed. Most of the argon flows out the unheated extensions during the test run to prevent oxygen from entering the hot graphite tube. Visual examination indicates that oxidation should not be a concern as long as sufficient purging is performed before and during experimentation.

The furnace temperature is computer controlled, using the standard PID algorithm in a commercially available data acquisition and control software package (Laboratory Technologies Corporation, 1994). An optical pyrometer views the center of the mid-partition from one end of the blackbody and provides temperature feedback to the control system. The thermal control system is capable of maintaining the indicated temperature within ±0.5 °C of the desired steady-state set point from 800 °C to 2200 °C.

**Instrumentation**

Various measurements were required to characterize the blackbody cavity. These included the temperature at the center of the partition in the middle of the blackbody (henceforth referred to as *blackbody temperature*), partition emissivity, electrical current passing through the blackbody assembly, axial blackbody surface temperature profiles, and location of the axial temperature sensor.

**Optical Pyrometers.**  Three optical pyrometers (Fig. 6) were utilized during the experimental characterization of the blackbody cavity. The control pyrometer and reference



**Figure 6.  Top View of Pyrometer and OFT Locations.**

4

pyrometer measured blackbody temperature. The third pyrometer, which included an emissivity measurement system, was used to measure the partition emissivity at both room temperature and at the test temperature.

The control and reference pyrometers were identical radiation pyrometers capable of measuring temperatures between 800 °C and 3100 °C. Their measurement area covers approximately one-quarter of the diameter of the blackbody partition. The response time of these pyrometers is 0.5 seconds for a step change from room temperature to test temperature. The control pyrometer was used by the control system to maintain stable temperatures and its calibration was accurate to within ±1 °C at 1100 °C. The reference pyrometer was calibrated at NIST prior to testing. The NIST calibration included a 95-percent confidence uncertainty of 0.7 °C at 1100 °C. The temperature measurements of the center partition measured by the reference pyrometer will be referred to as the *blackbody temperature* throughout this paper.

The third pyrometer included a system for measuring surface emissivity (Cameron, 1989) at both room temperature and test temperatures. The pyrometer measures emissivities from 0.1 to 1.00 by determining how much energy, from a low-power laser, was reflected off the center partition. This pyrometer could complete an emissivity measurement approximately once per second. These emissivity measurements are accurate to within ±0.01. The pyrometer operation is based on the assumption that the emissivity measurement is being taken on a diffuse reflecting surface at a temperature of less than 1500 °C.

**Optical Fiber Thermometer (OFT).** Axial surface temperature profiles of the blackbody cavity were obtained using an OFT, (Luxtron, 1990) with a 90° bend at the tip (Fig. 7). The OFT system includes a single crystal sapphire lightpipe, a fiber optic cable, and a receiving unit consisting of an optical detector and signal conditioning. The lightpipe is the only piece of the system which enters the blackbody cavity. The light is transmitted from the lightpipe to the receiving unit through the fiber optic cable. The receiving unit senses the
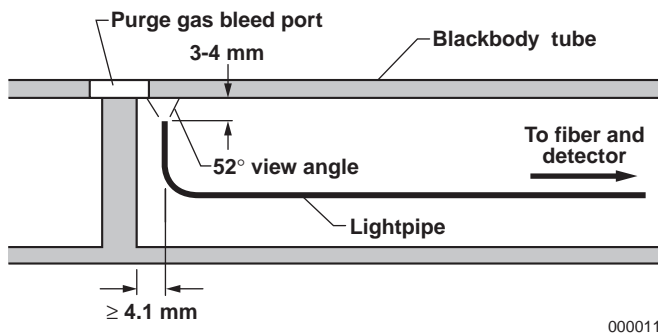
incoming infrared energy and converts that energy into a DC voltage proportional to temperature, which is routed to a data acquisition system.

The OFT system is capable of measuring temperatures from 400 °C to 1900 °C with a resolution of 0.4 °C. Response time of the OFT system is 0.04 seconds. The OFT was mounted on the slide track and crossbar assembly (see Fig. 6). The OFT mount (Fig. 8) was locally designed and built to include the capability of rotating the sensor to measure the axial temperature distribution at various locations around the interior circumference of the blackbody cavity. This mount held the tip of the sensor between 3 mm and 4 mm from the blackbody wall (Fig. 7). The axial temperature profiles were obtained by fixing the OFT at the desired angular location and then slowly inserting the OFT into the blackbody. The OFT was stopped at several axial locations as it was moved into the blackbody in order to obtain steady-state readings. The axial location of the sensing tip was measured using a deflection potentiometer connected to the crossbar.

During testing, we noticed that a significant amount of energy was entering the OFT through the bend in the sensor. This effect was obvious when the indicated temperature rose above the minimum reading of 400 °C by simply placing the OFT outside the entrance and in line with the hot blackbody with the sensor tip aimed at ambient surroundings, such as the walls or floor. The effect disappeared when the OFT sensor was moved away
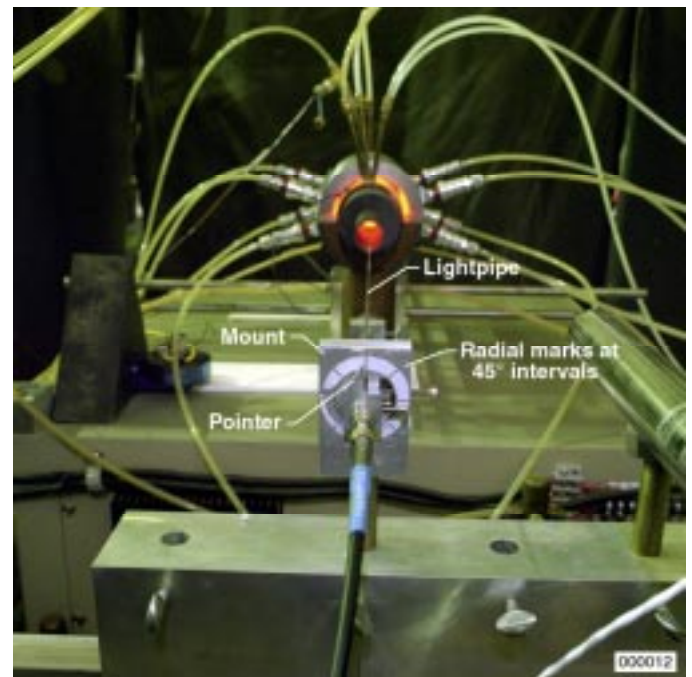


**Figure 7. OFT Insertion Geometry.**



**Figure 8. OFT and Mount.**

5

from the axis of the hot blackbody while still viewing the ambient surface.

A Monte Carlo ray trace analysis was performed on the OFT sensor to obtain a rough estimate of the energy traveling down the axis of the sensor, which entered through the bend instead of the sensing tip. The analysis included a model of the blackbody interior, which served as the emitting surface. This analysis demonstrated that the light entering the sensor at the bend was on the order of 10 percent of the total energy traveling down the axis of the OFT. Also, the analysis showed that this percentage remained essentially constant at all axial locations in the portion of the blackbody between the copper electrodes.

Some of the energy entering the bend was likely to be present, and thereby accounted for, during the manufacturers calibration process. Therefore, it was inappropriate to apply a 10-percent reduction to the total emissive power measured by the sensor. The total emissive power for a blackbody is represented by

$$E_{tot} = \sigma T^4 \tag{1}$$

A correction scheme was developed which utilized the known temperature (from the reference optical pyrometer) at the center partition to correct the OFT measurements. The OFT should indicate nearly the same temperature as the pyrometer when the OFT is located near the center partition. Assuming this to be the case, a correction factor can be determined from

$$F = \frac{E_{ref}}{E_{ind}} = \frac{(T_{ref})^4}{[T_{ind}(x = 4mm)]^4} \tag{2}$$

The corrected temperature for any axial location in the hot zone of the blackbody can then be obtained from

$$T_{corr}(x) = \{F[T_{ind}(x)]^4\}^{1/4} \tag{3}$$

The measurement uncertainty for the corrected temperature obtained when using equations (2) and (3) is taken to be ±5 °C. This uncertainty includes consideration of the uncertainties of the measurements used in the equations and the presence of temperature gradients within the blackbody, as demonstrated in the thermal analysis.

**OFT Position Measurement.** The position of the OFT sensing tip was measured using a deflection measurement potentiometer. The range of the device was 0 to 1080 mm with an accuracy of ±1.6 mm. Measurement response time was 60 microseconds. The deflection measurement potentiometer was mounted on the top of the calibration system power supply cabinet (Fig. 6). The spring-loaded string from the deflection measurement potentiometer was connected to the crossbar assembly. The measurement system was calibrated such that 0 mm was indicated when the OFT was in contact with the center partition.

**Electric Current Measurement.** The electrical current passing through the blackbody assembly was measured using a current transformer with an input-to-output reduction ratio of 1200:5. The output from the current transformer was connected to a current transducer, which converted the reduced current to a DC voltage. This DC voltage could then be acquired by the data acquisition system and converted into the value of the blackbody assembly current. The measurement uncertainty of the current transformer and transducer combination was ±13 amperes and the response time was 0.1 seconds.

**Measurement Uncertainty.** Uncertainties for the various measurements are summarized in Table 1. The uncertainties have been divided into two groups. The first group is the measurement uncertainty inherent in the sensor, shown on the top row of data. The second group is the uncertainty of the data acquisition systems measurement of the sensor output. The total uncertainty is obtained by the square-root-of-the-sum-of-the-squares method. All of these uncertainties are expressed in terms of engineering units appropriate for the particular measurement.

### Test Procedure

The test process began by assembling and installing the blackbody on the power supply electrode cradles. This assembly process included connecting hoses for cooling water and argon purge gas to the ports on the copper rings. The only difference in the assembly for the insulated and uninsulated tests was the installation of graphite felt and foil insulation between the

**Table 1: Measurement Uncertainty Summary at 1100 °C.**

| Source | Reference pyrometer, °C | Current, amperes | OFT, °C | Axial location, mm | Emissivity |
|---|---|---|---|---|---|
| Sensor | 0.7 | 13.0 | 5.0 | 1.6 | 0.01 |
| Data acquisition | 0.1 | 0.7 | 0.2 | 0.3 | N/A |
| Total | 0.7 | 13.0 | 5.0 | 1.6 | 0.01 |

blackbody and quartz tube for insulated tests. The pyrometers and OFT were then installed and aligned with the blackbody.

Tests of the insulated and uninsulated blackbody followed the same process once assembly was complete. Each test began by establishing cooling water and purge gas flow to the blackbody. Establishing cooling water flow was a simple matter of configuring valves and turning on the closed-loop water system. Argon purge gas was supplied from a standard 17.2 MPa tank. The initial argon flow rate was greater than 2 $m^3$/hr in order to blow air out of the system. Argon was forced into the central portion of the blackbody and between the blackbody and quartz tube by closing off the ends of the blackbody extensions. The extensions remained blocked for at least one minute. The total argon flow was then reduced to 0.28 $m^3$/hr, which was sufficient to maintain a slow flow of argon out of various openings in the blackbody assembly and prevent air from re-entering the assembly.

Once the cooling water and purge gas flows were established, the data acquisition and control software was started and the blackbody furnace was placed in manual power control. The manual power setting was manipulated to maintain a temperature rise rate of 3 °C to 5 °C per second until the measured temperature approached the desired test temperature. The control software was switched into automatic PID control once the measured temperature was within 25 °C of the desired test temperature. The control software was then allowed to stabilize control at the desired test temperature. The set point temperature was stabilized to within ±0.5 °C of the desired test temperature in less than 3 minutes.

Once the blackbody temperature was stabilized according to the control pyrometer, the blackbody temperature was checked with the NIST-calibrated reference pyrometer. These temperatures were measured on opposite sides of the center partition and were within ±0.4 °C, well within the uncertainty of the NIST pyrometer calibration. The NIST-calibrated pyrometer was then moved away from the blackbody axis in order to provide a clear view for the emissivity measuring pyrometer, and the emissivity measurement was taken.

Once the emissivity measurement was recorded, the ninety-degree-bend OFT was positioned in front of the blackbody. The initial angular position of the OFT sensing tip was pointing up (0° rotation), as shown in Fig. 8. The OFT was then slowly pushed into the blackbody while its indicated temperature and tip location were recorded by the data acquisition system. During the uninsulated test, which occurred early in the test program, the OFT was inserted into the blackbody with steady motion. Approximately 30 seconds elapsed between the time of first motion and when the sensing tip reached maximum depth. The sensor was left at maximum depth for approximately 6 seconds and then pulled out of the blackbody.

The insertion process for the insulated case was slightly different, in that the sensor was stopped for 5 to 10 seconds at several axial locations. The locations were nominally 142 mm, 136 mm, 129 mm, 117 mm, 91 mm, 66 mm, 40.6 mm, 15.3 mm, and 4.1 mm from the center partition. The slide track on which the OFT was mounted was pushed against a stop for the full insertion at 4.1 mm and this axial position was repeated within the measurement uncertainty previously stated. The slide track was manually positioned at marks representing the other axial locations and these locations were repeated within ±2 mm.

Insertions were performed in a clockwise direction every 45° around the circumference in both the uninsulated and insulated configurations. The sensor was rotated manually using the pointer and radial marks shown in Fig. 8 as guides.

## THERMAL ANALYSIS

Numerical thermal analyses of the insulated and uninsulated blackbody configurations were developed to aid in the study and understanding of the relevant heat transfer mechanisms present in the calibration system. This section discusses the software used, the model geometry and grid, the boundary conditions and assumptions applied to the model, how heat generation was incorporated, and the material properties used in the analyses.
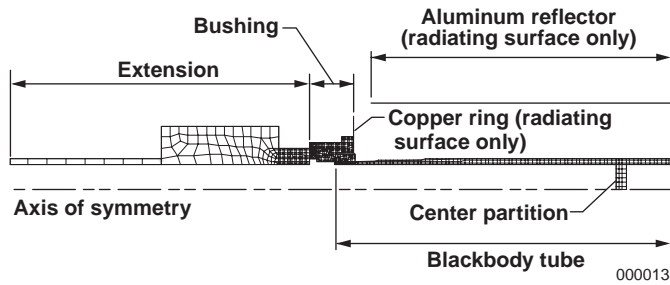
### Software

Numerical models of the blackbody assembly were developed, for both the insulated and uninsulated configurations, using commercially available thermal analysis software (MacNeal-Schwendler Corporation, 1999). The software includes a user interface for model generation and a radiation view factor analysis program in addition to a thermal solver. The thermal solver converts the model mesh into a thermal resistor-capacitor network and uses a weighted explicit-implicit finite difference scheme to generate the solution. Details of the numerical solution technique may be found in Volume 1, Chapter 7 of the MacNeal-Schwendler Corporation manual.

### Geometry and Grid

The numerical model geometry was input as a two-dimensional cross section, bounded by the centerline axis (at the bottom) and including both the left and right cavities of the blackbody assembly. Figure 9 shows the left side of the model. The graphite tube, end cap bushings, and extensions were fully modeled. The aluminum reflector and copper rings were modeled as constant temperature surfaces in the uninsulated model. Options selected in the thermal analysis software instruct the solver to interpret the geometry as a thin slice of an axisymmetric object and compute the radiation and conduction heat transfer accordingly.

The mesh shown in Fig. 9 represents the initial mesh used for both the insulated and uninsulated cases. The node spacing in the blackbody wall was nominally 2 mm axial by 1 mm radial. The spacing was reduced to 1 mm axial at the connection to the

**Figure 9. Thermal Analysis Model, Left Side of Blackbody.**

bushing. The radial spacing was varied as required in the tapered region of the blackbody to maintain 4 nodes in the radial direction. Node spacing was 2 mm x 2 mm in the center partition. The bushings, where higher thermal gradients were expected, were meshed with a nominal 1 mm by 1 mm node spacing. A variable node spacing was used in the mesh of the end extensions. This mesh was approximately 1 mm by 1 mm near the bushings and expanded to approximately 9 mm x 9 mm as distance from the bushings increased.

**Insulated Model.** Graphite felt surrounds the graphite tube in the insulated configuration but was not included in the model geometry.   The effect of the insulation was modeled as an adiabatic boundary condition on the exterior tube wall and reduced electric current passing through the graphite tube, as discussed below.

**Uninsulated Model.** The water-cooled copper ring at each end cap and the water-cooled aluminum reflector were represented as surfaces at fixed temperatures for the uninsulated model geometry and mesh.   The copper caps and aluminum reflector were included as boundaries in the model to properly define the radiant heat transfer from the external surface of the uninsulated graphite tube.

**Mesh Refinement.** Grid refinement was performed in the blackbody node spacing in order to verify grid-independent results. The blackbody mesh was reduced to a nominal 1 mm axial by 1 mm radial node spacing throughout the blackbody. Reduction of the radial node spacing in the tapered region of the tube was maintained. Mesh refinement was not performed on the bushings and end extensions. Variations resulting from mesh refinement in the axial temperature profile were less than 2.5 °C for the uninsulated case and less than 1 °C for the insulated case. These variations are negligible (<0.25 percent) compared to the nominal 1100 °C blackbody temperature and are within experimental measurement uncertainty. Therefore, the nominal 2 mm axial mesh was used to generate data for this paper in order to reduce computation time.

## Modeling Assumptions

Certain assumptions had to be made in the thermal models. Simplifying assumptions were made concerning thermal contact resistance, effect of the quartz tube, temperature of the reflector and copper rings, and internal convection of the blackbody cavity.

**Thermal Contact Resistance.** Thermal contact resistance is a significant factor affecting the conduction heat transfer at the material interfaces in both end caps. These interfaces include blackbody-to-bushing, bushing-to-copper ring, and between bushing components. However, it is extremely difficult to make high-quality estimates of contact resistance. For this analysis, contact resistance has been neglected and the copper-bushing contact temperature was varied as required to match the experimental temperature measurements at the ends of the graphite tube. It was assumed that this technique would sufficiently account for the effect of contact resistance on the heat transfer through the bushing.

**Effect of Quartz Tube.** The quartz tube, being essentially transparent to infrared radiation, was assumed to have little effect on the radiant heat transfer between the external surface of the graphite tube and the reflector and copper end caps in the uninsulated configuration. Likewise, the quartz was considered to have no effect on the heat transfer from the graphite tube in the insulated configuration. Therefore, the quartz tube was not included in either the insulated or uninsulated model.

**Reflector and Copper Ring Temperature.** The aluminum reflector and copper rings were water cooled and provided the external radiation boundary for the graphite tube in the uninsulated configuration. The temperature distribution on these components was modeled as isothermal and at the nominal cooling-water temperature (40 °C).

**Blackbody Cavity Internal Convection.** Convection inside the blackbody cavity was assumed to be negligible based on experimental observations. The argon flow-rate input at each end cap was 0.14 m$^3$/hr for all runs. Because of the lack of resistance to flow, most of the argon exits through the extension tubes. Therefore, forced convection is not expected to be significant in the blackbody cavity. In addition, examination of circumferential temperature variations showed insignificant changes, verifying that natural convection was also insignificant.

## Heat Generation

Heat was input into the insulated and uninsulated thermal models by using volumetric heat generation. The thermal solver computed the heat generation per unit volume based on the given total current passing through the blackbody assembly, the local geometry of the assembly, and the electrical resistivity. The total electric current passing through the assembly was

measured during each test and the measured value was used in the model. The models included temperature-dependent electrical resistivity for the ATJ graphite tube and constant electrical resistivity for the pyrolytic graphite and carbon-carbon components. The equation used in the model for power dissipated per unit volume was

$$\frac{P}{V} = \frac{I^2 R}{V} \qquad (4)$$

However,

$$R = \frac{\rho L}{A} \qquad (5)$$

and

$$V = LA \qquad (6)$$

So,

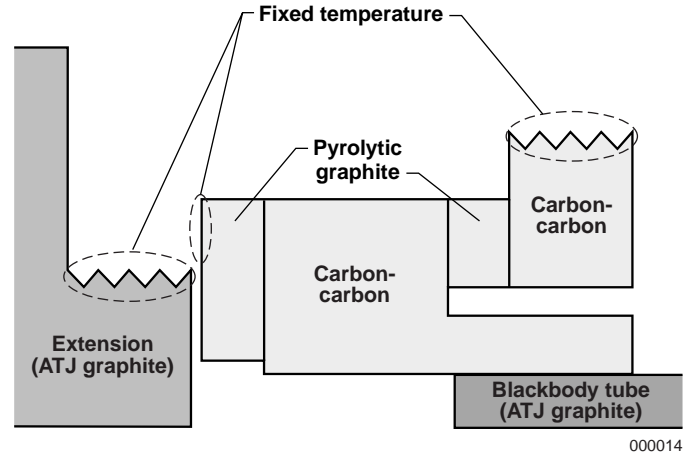$$\frac{P}{V} = \frac{\rho I^2}{A^2} \qquad (7)$$

Here 'A' represents the total area through which current flows in the actual hardware. The area and electrical resistivity were computed at each node where heat generation was defined.

There were two areas in each end cap where the electric current flowed from the copper ring into the bushing. The total current was divided between these two areas in proportion to the local contact area between the bushing and copper ring.

**Insulated Model Adjustments.** Some of the electric current passing through the blackbody assembly passed through the graphite felt and foil insulation instead of the graphite tube in the insulated configuration. Measurement of the actual currents passing through the graphite tube and insulation was not possible because the configuration of the system and the extreme temperatures involved did not allow it. The current passing through the graphite tube was reduced as required in the insulated model in order to obtain agreement with experimental results. Reasonable agreement, within 6.5 °C, was obtained between the numerical and experimental results with 49.3 percent of the total measured current passing through the insulated portion of the blackbody.

## Boundary Conditions

The thermal boundary conditions in the blackbody assembly were symmetric about the center partition for the steady-state analysis presented in this paper. However, the entire assembly was modeled in order to support future work, which would involve transient, asymmetric conditions. Modes of heat transfer common to both the insulated and uninsulated configurations include: (1) fixed isothermal temperatures where the bushings and extensions contact the copper rings (Fig. 10), (2) radiation



**Figure 10. Bushing Geometry Detail.**

on the interior of the blackbody, bushings, and extensions, and (3) natural convection on the exterior of the extensions.

Unique boundary conditions existed on the external surface of the graphite tube for uninsulated and insulated configurations. The model of the uninsulated configuration included radiation exchange between the graphite tube and the water-cooled copper rings and aluminum reflector. The adiabatic wall boundary condition on the external surface of the graphite tube was used for the insulated model.
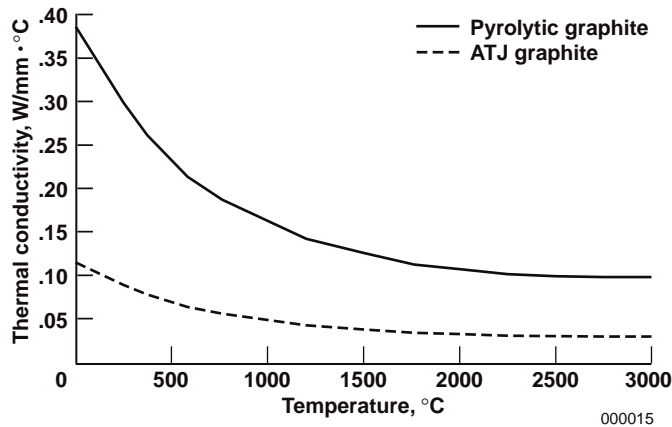
**Bushing-Copper Ring Boundary Temperature.** A fixed isothermal temperature boundary condition was enforced at the points where the bushings contacted the copper rings in each end cap. These temperatures were adjusted as required in both the insulated and uninsulated models in order to attain agreement between the experimentally and numerically determined tube surface temperatures. The lack of thermal contact resistance in the thermal models resulted in these boundary condition temperatures being set artificially high.

**External Surface Radiation from the Graphite Tube (Uninsulated Blackbody).** Radiation exchange was included in the uninsulated model between the exterior of the blackbody and the copper rings and aluminum reflector. The emissivity values for the copper rings and aluminum reflector were adjusted, within literature-reported values, to obtain numerical results in good agreement with experimental results. Both the copper and aluminum surfaces had significant surface oxidation and their emissivities were assumed to be the same. Ring and reflector emissivity of 0.26 produced numerical results within 5.2 °C of the measured axial temperature. The emissivity of 0.26 is within the range presented in Siegel and Howell (1992) for oxidized aluminum.
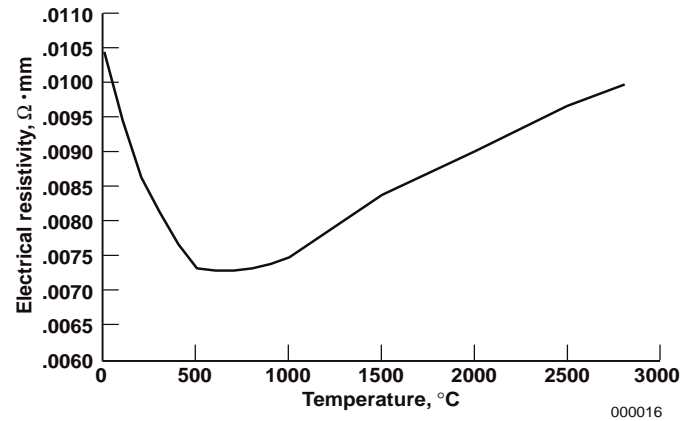
**Adiabatic Wall (Insulated Blackbody).** The adiabatic wall boundary condition was enforced on the exterior of the graphite tube in the insulated configuration model. An insignificant amount of heat was expected to flow radially through the insulation due to the thermal resistance of the insulation and heating of the insulation by a portion of the electric current passing through the blackbody assembly.

## Material Properties

Properties, including thermal conductivity and electrical resistivity, for the various materials involved (Fig. 10) were obtained from manufacturers data whenever possible. Thermal conductivity and electrical resistivity for ATJ graphite were available from the manufacturer as a function of temperature throughout the range of interest (Fig. 11 and 12). The manufacturer of the carbon-carbon composite provided thermal conductivity data from room temperature to 120 °C and electrical resistivity data at room temperature (Table 2). The carbon-carbon thermal conductivity value at 120 °C was used in the analysis. Values for the thermal conductivity and electrical resistivity of pyrolytic graphite at room temperature were obtained from Clauser et al. (1963), and are summarized in Table 2. Temperature dependence of pyrolytic graphite thermal conductivity (Fig. 11) followed the same relative curve as ATJ graphite.

**Figure 12. Electrical Resistivity of ATJ Graphite.**

**Figure 11. Thermal Conductivity for ATJ Graphite and Pyrolytic Graphite.**

**Table 2: Material Thermal Conductivity and Electrical Resistivity.**

| Material | Thermal conductivity (W/mm ·°C) | Electrical resistivity (Ω ·mm) |
|---|---|---|
| ATJ Graphite | See Fig. 11 | See Fig. 12 |
| Carbon-Carbon (parallel to laminate at 120 °C) | 0.0865 | 0.00889 |
| Carbon-Carbon (perpendicular to laminate at 120 °C) | 0.04152 | 0.02159 |
| Pyrolytic Graphite (parallel to grain) | See Fig. 11 | 0.005 |

The emissivity of the ATJ blackbody center partition was measured as part of the test and was used as the emissivity for all graphite radiating surfaces. Published values (Siegel and Howell, 1992) were used for initial estimates for the aluminum reflector and copper ring emissivity (Table 3). The copper and

**Table 3: Material Emissivity.**

| ATJ Graphite (measured, used for all graphite components) Emissivity: 0.88 – 0.91 | Oxidized Aluminum (Siegel and Howell, 1992) Emissivity: 0.20 – 0.31 | Copper (depending on level of polish and oxidation) (Siegel and Howell, 1992) Emissivity: 0.15 – 0.78 |
|---|---|---|

10

aluminum emissivities are heavily dependent on the degree of oxidation, so they are used only as a guide. Measurement of the highly specular copper and aluminum emissivities was not possible because the available emissivity measuring equipment required diffuse reflection for proper operation.

## RESULTS

This section discusses both the experimental and numerical analysis results. These results are discussed and compared for both the uninsulated and insulated blackbody configurations.

### Experimental Results

**Uninsulated Configuration.** The corrected measured axial temperature profiles taken with the OFT at 0°, 90°, 180°, and 270° rotation during the uninsulated test are shown in Fig. 13. The temperature profiles are nearly isothermal up to 20 mm from the partition and then drop off slightly to around 70 mm from the partition, which is the approximate location where the graphite tube begins to taper. There is another essentially isothermal region between 70 mm and 100 mm after which a sharp temperature decrease begins. The blackbody walls remain within 20 °C of the nominal blackbody temperature, 1100 °C, up to approximately 100 mm from the center partition.
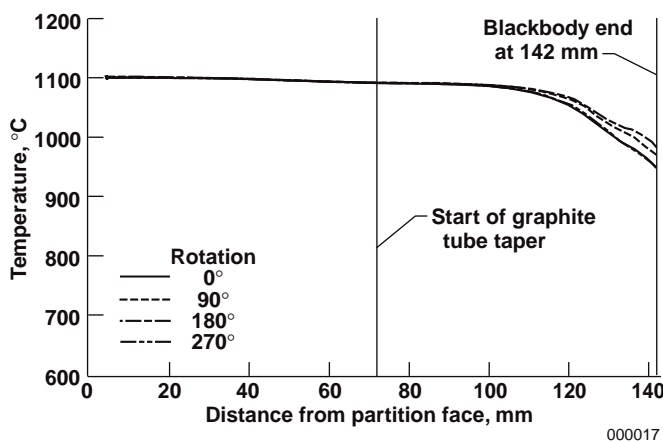
A slight temperature decrease of 3.5 °C was observed in the OFT measurements taken at 0° position at the 4.1 mm location. This decrease resulted from the presence of the purge gas bleed slot at the top center of the graphite tube. This observation was consistent with findings in Abdelmessih (1998). The end of this slot is 2 mm from the partition and just comes into the view angle of the OFT centered at approximately 4 mm from the partition (Fig. 7).

The blackbody was held at a constant temperature to within ±0.1 °C as indicated by the control pyrometer. The temperature indicated by the NIST-calibrated reference pyrometer, which viewed the end of the blackbody measured by the OFT, was within ±0.3 °C of the temperature indicated by the control pyrometer. The emissivity of the center partition measured during uninsulated tests varied from 0.88 to 0.90. A value of 0.89 was used as the graphite emissivity in the thermal analysis. The measured electric current passing through the blackbody was 602 amperes.
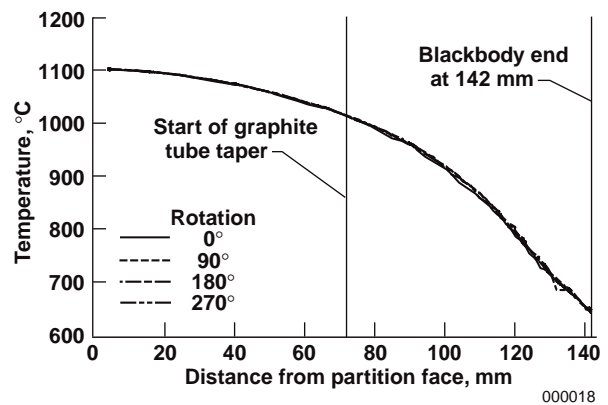
**Insulated Configuration.** The corrected measured axial temperature profiles taken with the OFT at 0°, 90°, 180°, and 270° rotation during the insulated test are shown in Fig. 14. These profiles show the typical nonlinear temperature distribution expected from heat transfer that is dominated by heat generation and conduction.

A decrease in the 0° position temperature at the 4.1 mm location was also observed in the insulated tests. The decrease was approximately 2.5 °C, 1 °C less than that observed in the uninsulated test. This is appropriate since the OFT would view hot insulation wrapped around the blackbody through the bleed slot, but the OFT would view the cool aluminum reflector through the slot in the uninsulated case.

The insulated blackbody temperature was held constant to within ±0.1 °C as measured by the control pyrometer. The NIST-calibrated reference pyrometer indicated a temperature within 0.4 °C of the control temperature value. The measured emissivity of the partition during the 1100 °C insulated test was 0.91. This value was used in the thermal analysis of the insulated blackbody. The measured total electric current passing



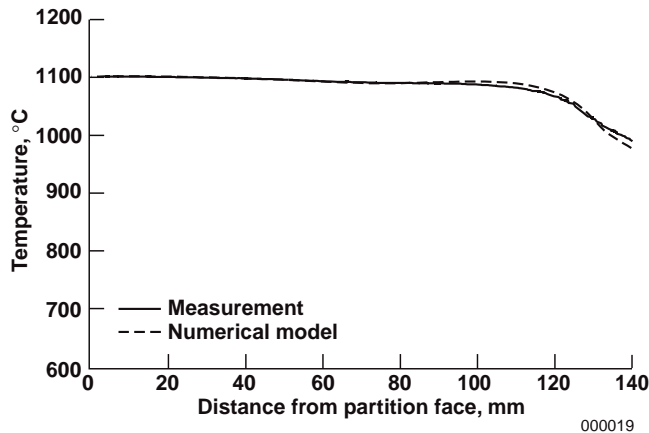**Figure 13. Uninsulated Blackbody Axial Temperature Distribution.**



**Figure 14. Insulated Blackbody Axial Temperature Distribution.**

through the blackbody assembly was 334 amperes. This value includes current that passed through the insulation and the graphite tube.

### Thermal Analysis Results

**Uninsulated Model.** The numerical results from the uninsulated blackbody model were brought into agreement with experimental results by adjusting the reflector emissivity and the bushing-copper ring boundary temperature. The computed temperatures are within ±3 °C at locations less than 90 mm from the center partition (Fig. 15). The maximum difference between computed and measured temperatures between 90 mm and 130 mm from the partition is less than 7 °C. Temperature differences are less than 15 °C from 130 mm to the end of the graphite tube at 141.8 mm.
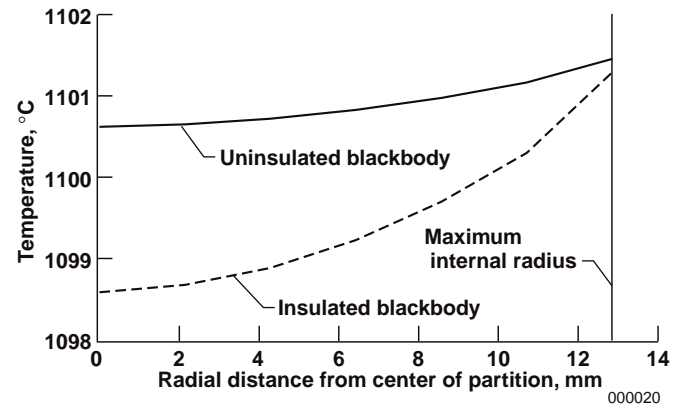


**Figure 15.   Uninsulated Blackbody Axial Temperature Distribution from Experimental Measurement and Numerical Model.**

The computed temperature profile includes a hump between 75 mm and 110 mm from the partition that is not found in the experimental data. Axial mesh density has been ruled out as a cause of this anomaly since doubling the axial mesh density had minimal effect on the magnitude of the increase. The external blackbody radiation boundary condition has been found to have a significant impact on the magnitude of the increase. A decrease of 0.02 in the reflector emissivity virtually eliminated the hump, reducing it to only 0.5 °C. However, decreasing the reflector emissivity increased the partition temperature 15 °C above the measured result. Small changes within manufacturing tolerances in the blackbody taper, particularly in the heat generation calculations, have also had significant effect on the increase. These small changes in the heating calculation have been shown to change the magnitude of the increase by at least 5 °C. The factors affecting the anomalous temperature increase
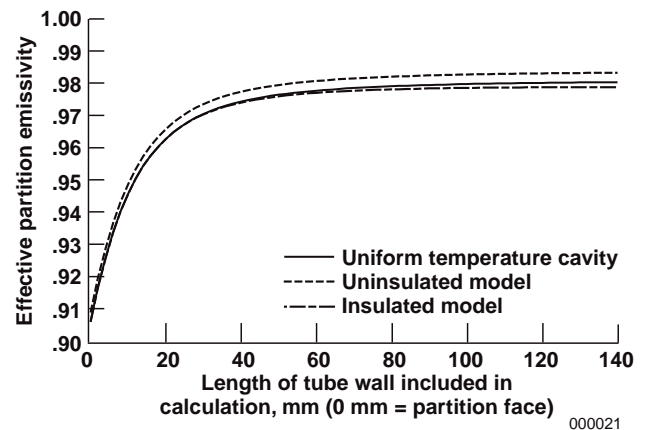
have been adjusted to minimize the deviation from the measured temperature profile.

The thermal analysis provided insight regarding the uniformity of the center partition temperature. The center wall temperature varied less than 1 °C in the uninsulated model (Fig. 16).



**Figure 16.   Center Partition Temperature Distribution.**

The thermal analysis data may also be used to estimate the effective emissivity of the center partition. For this discussion, effective emissivity is defined as the total energy emitted from and reflected by the center partition divided by the energy that would be emitted if the partition were a perfect emitter. The effective emissivity depends on the length of the tube's cylindrical wall included in the calculation. Figure 17 shows the variation in computed effective emissivity as a function of the length of tube wall included in the calculation. The effective emissivity computed for the uninsulated model is within
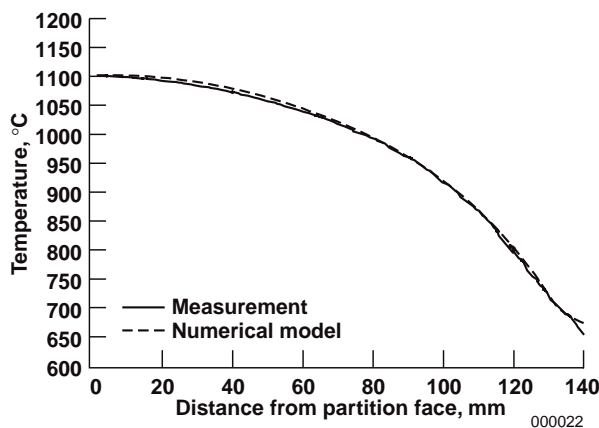


**Figure 17.   Effective Emissivity Computation.**

0.1 percent of its final value of 0.983 when including 85 mm of the tube wall extending from the partition. This indicates that temperature variations beyond 85 mm will have little effect on the partition effective emissivity. Also note that the effective emissivity computed for the model is slightly higher than that calculated for a perfectly isothermal blackbody cavity at 1100 °C. This results from the fact that the temperatures near the center partition, as computed in the model, were slightly higher than the ideal condition.

**Insulated Model.** The bushing-copper ring contact temperature and the portion of electrical current passing through the blackbody cylinder were adjusted to bring the insulated blackbody model into agreement with the experimental results. This adjustment process resulted in 49.3 percent of the total measured current actually passing through the blackbody and a bushing-copper ring contact boundary temperature of 645 °C. The remaining 50.7 percent of the current is assumed to travel through the graphite felt insulation which surrounds the blackbody. The model reproduced experimental measurements within ±5 °C (Fig. 18), except at the blackbody-bushing interface. The model produced temperatures 20 °C above the measured results in this region as a result of the complex heat transfer and electrical current flow at the contact boundary between the graphite tube and bushing.

The variations in center partition temperature were greater in the insulated model than they were in the uninsulated model. Figure 16 shows the insulated model partition temperature varied nearly 3° from the center to the outer edge. This is because of the lower temperatures in, and therefore lower energy arriving from, the blackbody cavity walls.



**Figure 18.   Insulated Blackbody Axial Temperature Distribution from Experimental Measurement and Thermal Model.**

The cooler temperatures in the insulated case led to a somewhat lower effective partition emissivity as well. The effective partition emissivity was 0.979 when using the entire graphite tube in the calculation. The lower value is a result of the cooler temperatures in the insulated blackbody as the end of the graphite tube is approached. The effective partition emissivity was within 0.1 percent of its final value after 74 mm of the tube had been included in the calculation.

**Sensitivity Analysis.** An analysis has been performed to assess the sensitivity of the temperature profiles computed in the insulated and uninsulated models to changes in various parameters used in the thermal model. Table 4 shows the parameters studied, the variation in each parameter which was applied to each model, and the resulting maximum change in the axial temperature distribution for both the insulated and uninsulated cases. The amount of variation for blackbody emissivity and total electrical current was based on measurement uncertainty. Engineering judgement was used to choose reasonable variations in other parameters.

The axial temperature distributions are most sensitive to the total current passing through the blackbody. Both electrical resistivity and reflector emissivity produced significant changes in the computed axial temperatures of the uninsulated blackbody. The maximums shown in Table 4 for these two parameters occurred at the center partition. However, the temperature computed near the mouth of the blackbody varied only ±3.5 °C and less than ±1 °C for the variation of electrical resistivity and reflector emissivity, respectively.

The bushing-copper ring boundary temperature variation of ±25 °C caused changes in the computed temperature at the mouth of the blackbody of ±21 °C and ±25 °C for the uninsulated and insulated cases, respectively. The partition temperature changed less than ±1 °C when this boundary condition was changed by ±25 °C.

The change in blackbody emissivity resulted in a relatively small change in uninsulated blackbody temperatures. The maximum temperature change for the variation of this parameter occurred near the center partition.

The change in uninsulated blackbody thermal conductivity resulted in a nearly insignificant temperature change, which had its maximum near the mouth of the blackbody. The change caused by variation of this parameter was only about 0.3° C at the center partition.

The model of the insulated configuration demonstrated significant sensitivity to other parameters, such as thermal conductivity, electrical resistivity, and bushing-copper ring boundary temperature, which influence the heat generation and conduction within the model. The changes induced by these parameters were of the same order of magnitude throughout the blackbody cavity.

13

**Table 4: Sensitivity of Blackbody Temperature to Changes in Various Parameters.**

| Property or Boundary Condition | Variation | Maximum Change | | | |
| --- | --- | --- | --- | --- | --- |
| | | Uninsulated | | Insulated | |
| | | Location | $\Delta T$, °C | Location | $\Delta T$, °C |
| Blackbody thermal conductivity | ±5.0 percent | mouth | ±1.0 | partition | ±17.00 |
| Electrical resistivity | ±5.0 percent | partition | ±19.0 | partition | ±25.00 |
| Blackbody emissivity | ±2.2 percent | partition | ±4.5 | partition | ±0.18 |
| Reflector emissivity | ±8.5 percent | partition | ±15.0 | | |
| Total current | ±26 amperes | partition | ±32.0 | partition | ±75.00 |
| Bushing-copper ring boundary temperature | ±25.0 °C | mouth | ±21.0 | mouth | ±25.00 |

The insulated model was nearly insensitive to small changes in blackbody emissivity. A blackbody emissivity change of 0.02 (about 2 percent of the nominal value), caused <0.2 °C change in the computed axial temperatures.

## CONCLUDING REMARKS

A cylindrical, dual-cavity blackbody has been characterized through experimental measurements and numerical models for steady-state operation at 1100 °C. Two hardware configurations were explored. The first configuration, recommended for operation at temperatures below 1100 °C, allowed the exterior of the graphite tube to radiate to a water-cooled aluminum reflector. The second configuration, employed for calibration at temperatures above 1100 ° C, accounted for graphite felt insulation wrapped around the graphite tube.

Measurement of the axial temperature profile in the uninsulated configuration revealed a nearly isothermal section extending 20 mm from the center partition. Tube wall temperatures remained within 20 °C of the center partition temperature up to 100 mm from the partition. The axial temperature distribution in the insulated configuration was much less isothermal.

Measurements of the axial temperature profile, at preset axial locations, were taken every 45° around the inner circumference of the blackbody cavity. These temperature measurements confirm that internal natural and forced convection are essentially insignificant in both the insulated and uninsulated models.

The numerical models of the steady-state operation of the blackbody, in both the insulated and uninsulated configurations, have been tuned to experimental results. The models for both configurations capture the relevant heat transfer mechanisms and produce computed axial temperature profiles within 8 °C of the measured results.

The heat transfer mechanisms with significant impact on the uninsulated model are (1) radiation exchange affecting the external surface of the graphite tube, and (2) heat generation in the graphite tube. Variations of the properties and boundary conditions affecting conduction and radiation in the interior of the blackbody had little effect on the blackbody temperature.

Variations in the properties and boundary conditions related to heat generation and conduction had the largest impact on the calculation of blackbody temperature for the insulated model. The effect of radiation in the insulated model was relatively small.

The computed axial temperature distributions, as well as the computation of temperature gradients in the center partition, enabled the calculation of the effective partition emissivity. The effective partition emissivity in both the insulated and uninsulated configurations was approximately 0.98. This value is nearly identical to the value computed for a perfectly isothermal blackbody cavity.

The steady-state experiments and thermal models described in this paper provide a sound foundation for additional studies of the blackbody calibration system. It is recommended that the work presented in this paper be extended to the full range of operational temperatures from 800 °C to 2200 °C. Also, models of the transient insertion of the reference heat flux gage into the blackbody cavity, if explored, could lead to quantification of the uncertainties involved in that process.

## ACKNOWLEDGMENT

14

## REFERENCES

Abdelmessih, A. N., 1998, "Experimental Measurements of Temperature and Heat Flux in a High Temperature Black Body Cavity," NASA Technical Reports, NGT 2-52212, Document ID 19990021026, PP A:1-3.

Cameron, E. S., 1989, "Laser Assisted Remote Temperature Measurement," Optomechanical Design of Laser Transmitters and Receivers, SPIE Vol. 1044, pp. 155 – 162.

Clauser, H. R., Fabian, R., Peckner, D., and Riley, M. W., 1963, *The Encyclopedia of Engineering Materials and Processes*, Reinhold Publishing Corp., New York, New York.

Grosshandler, W. L,. and Blackburn, D., 1997, "Development of a High Flux Conduction Calibration Apparatus," HTD-Vol. 353, Proceedings of the ASME Heat Transfer Division, V. 3, pp. 153–158.

Holmberg, D., Steckler, K,. Womeldorf, C,. and Grosshandler, W., 1997, "Facility for Calibrating Heat Flux Sensors in a Convective Environment," HTD-Vol. 353, Proceedings of the ASME Heat Transfer Division, V. 3, pp. 165 – 171.

Holmberg, D. G., Womeldorf, C. A., and Grosshandler, W. L., 1999, "Design and Uncertainty Analysis of a Second-Generation Convective Heat Flux Calibration Facility," HTD-Vol. 364, Proceedings of the ASME Heat Transfer Division, V. 4, pp. 65 – 70.

Jiang, S., Horn, T. J., and Dhir, V. K., 1998, "Numerical Analysis of a Radiant Heat Flux Calibration System," HTD-Vol. 361, Proceedings of the ASME Heat Transfer Division, V. 5, pp. 609 – 616.

Laboratory Technologies Corporation, 1994, *LABTECH Data Acquisition and Process Control Software, Windows User's Guide*, Wilmington, Massachusetts.

Luxtron Inc., 1990, *Accufiber Models 10 &100 Optical Fiber Thermometers Manual*, Santa Clara, California.

MacNeal-Schwendler Corporation, 1999, *MSC/PATRAN THERMAL Users Guide*, Volumes 1 and 2, Software Version 8.5 Online Documentation.

Murthy, A. V., Tsai, B. K., and Saunders, R. D., 1997, "Radiative Calibration of Heat Flux Sensors at NIST – An Overview," HTD-Vol. 353, Proceedings of the ASME Heat Transfer Division, V. 3, pp. 159 - 164.

Siegel, R., and. Howell, J. R., 1992, *Thermal Radiation Heat Transfer*, 3rd edition, Hemisphere Publishing Corporation, Washington, D.C.

Thermogage Inc., 1991, *Thermogage Operation Manual for Model 48 kW Calibration Furnace*, Frostburg, Maryland.

# REPORT DOCUMENTATION PAGE

Form Approved
OMB No. 0704-0188

| 1. AGENCY USE ONLY (Leave blank) | 2. REPORT DATE<br>August 2000 | 3. REPORT TYPE AND DATES COVERED<br>Technical Memorandum |
|---|---|---|

**4. TITLE AND SUBTITLE**

Experimental and Numerical Characterization of a Steady-State Cylindrical Blackbody Cavity at 1100 Degrees Celsius

**5. FUNDING NUMBERS**

WU 522-32-24-E8-RS-00-000

**6. AUTHOR(S)**

Thomas J. Horn and Amanie N. Abdelmessih

**7. PERFORMING ORGANIZATION NAME(S) AND ADDRESS(ES)**

NASA Dryden Flight Research Center
P.O. Box 273
Edwards, California 93523-0273

**8. PERFORMING ORGANIZATION REPORT NUMBER**

H-2403

**9. SPONSORING/MONITORING AGENCY NAME(S) AND ADDRESS(ES)**

National Aeronautics and Space Administration
Washington, DC 20546-0001

**10. SPONSORING/MONITORING AGENCY REPORT NUMBER**

NASA/TM-2000-209022

**11. SUPPLEMENTARY NOTES**

Presented at 34th National Heat Transfer Conference, Pittsburgh, Pennsylvania, August 20–22, 2000, paper NHTC2000-12140. Dr. Abdelmessih is an Associate Professor, Mechanical Engineering Department at St Martin's College, Lacey, Washington and a participant in the NASA/ASEE Summer Faculty Fellowship Program.

**12a. DISTRIBUTION/AVAILABILITY STATEMENT**

Unclassified—Unlimited
Subject Category 34

This report is available at http://www.dfrc.nasa.gov/DTRS/

**12b. DISTRIBUTION CODE**

**13. ABSTRACT (Maximum 200 words)**

A blackbody calibration furnace at the NASA Dryden Flight Research Center is used to calibrate heat flux gages. These gages are for measuring the aerodynamic heat flux on hypersonic flight vehicle surfaces. The blackbody is a graphite tube with a midplane partition which divides the tube into two compartments (dual cavities). Electrical resistance heating is used to heat the graphite tube. This heating and the boundary conditions imposed on the graphite tube result in temperature gradients along the walls of the blackbody cavity. This paper describes measurements made during steady-state operation and development of finite-difference thermal models of the blockbody furnace at 1100 °C. Two configurations were studied, one with the blackbody outer surface insulated and the other without insulation. The dominant modes of heat transfer were identified for each configuration and the effect of variations in material properties and electric current that was passed through the blackbody were quantified.

**14. SUBJECT TERMS**

Blackbody calibration furnace, Heat flux calibration, Heat transfer, Numerical thermal analysis, Temperature measurement

**15. NUMBER OF PAGES**
21

**16. PRICE CODE**
A03

| 17. SECURITY CLASSIFICATION OF REPORT | 18. SECURITY CLASSIFICATION OF THIS PAGE | 19. SECURITY CLASSIFICATION OF ABSTRACT | 20. LIMITATION OF ABSTRACT |
|---|---|---|---|
| Unclassified | Unclassified | Unclassified | Unlimited |